

DFT-based *ab-initio* study of half-Heusler KCaP compound

Y. MOGULKOC^{a*}, Y.O. CİFTÇİ^b, G. SURUCU^{c,d,e}

^aDepartment of Physics Engineering, Ankara University, 06100, Tandogan, Ankara, Turkey

^bDepartment of Physics, Gazi University, 06500, Teknikokullar, Ankara, Turkey

^cAhi Evran University, Department of Electric and Energy, 40100, Kirsehir, Turkey

^dMiddle East Technical University, Department of Physics, 06800, Ankara, Turkey

^eGazi University, Photonics Application and Research Center, 06500, Ankara, Turkey

An *ab-initio* study of structural, elastic, electronic and optical properties of KCaP compound with space group $F\bar{4}3m$ have been reported using the plane-wave pseudo-potential technique based on density functional theory under pressure effect. The elastic anisotropy of compound is investigated in terms of Poisson's ratio, shear modulus and Young's modulus with pressure effect. The electronic band structure calculations and charge densities are obtained. Optical properties are also investigated and refraction index, extinction coefficient, reflectivity and loss function of KCaP compound are determined.

(Received October 26, 2016; accepted February 12, 2018)

Keywords: Ab-initio, Half-Heusler, Elastic properties, Electronic properties, Optical properties

1. Introduction

The investigations on optoelectronic and semiconductor technologies, half-Heusler (or semi-Heusler) compounds are novel materials for the improvement of these types of technologies such as laser diodes, thin film solar cells, buffer layer materials. Generally, half-Heusler compounds XYZ crystallize in a non-centrosymmetric structure corresponding to the space group $F\bar{4}3m$ (space number: 216) [1]. Recently, the half-Heusler compounds have had considerable interest due to their potential applications, such as thermoelectrics, green energy-related fields and spintronics [2]. The temperature dependence of electrical conductivity, Seebeck and Hall coefficients, and thermal conductivity of Nb-doped MNiSn ($M = \text{Ti, Zr}$) half-Heusler compounds were investigated at different temperatures, ranging from room temperature to 1000 K by Muta et al. [3]. The half-Heusler compounds have thermo-electrical properties. Recently, the enhancing of the thermoelectric performance of half-Heusler compounds are attracted the interest of nanotechnology applications. Recent studies for half-Heusler compounds are briefly reviewed by Xie and his friends [4]. Kieven and Klenk present their first principles calculations results in order to find potential half-Heusler materials to use in optoelectronic devices and defined the interesting materials [5]. We also consider and predict the half-Heusler compound KCaP is the most interesting material to investigate due to its convenient elastic, electronic, optical and vibrational properties.

Preferred configurations with semiconductor materials are compared for the different half-Heusler compounds by Gruhn [6]. The analysis of lattice parameters, band gaps and static dielectric constants of half-Heusler compounds at ambient pressure are investigated and demonstrated as new candidates for the optoelectronic devices by Mehnane et al. [7]. The structural, electronic and optical properties of half-Heusler compounds of I-II-V and I-III-IV types using first principles calculations based on the density functional theory by Kacimi et al. [8]. Here, we have investigated, presented and compared the structural, elastic, electronic, optical and vibrational properties of as a selected half-Heusler compound KCaP. In addition to such of these properties, pressure effect is also considered for calculations.

2. Model and Method

The half-Heusler compounds are composed with ternary XYZ has a 1:1:1 stoichiometry, its space group is $F\bar{4}3m$ and Pearson symbol is $C1_b$. The half-Heusler compounds have eight valence electrons, including a large number of semiconductors with energy gaps vary in a wide range [9].

The crystal structure of KCaP half-Heusler compound is shown in Fig. 1 with Wyckoff positions of atoms that are located as K (0.5, 0.5, 0.5); Ca (0.0, 0.0, 0.0); and P (0.25, 0.25, 0.25).

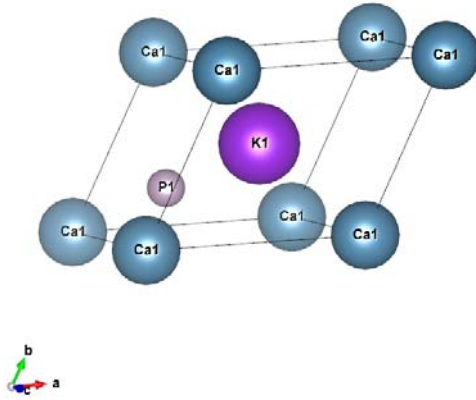


Fig. 1. Crystal structure of KCaP compound

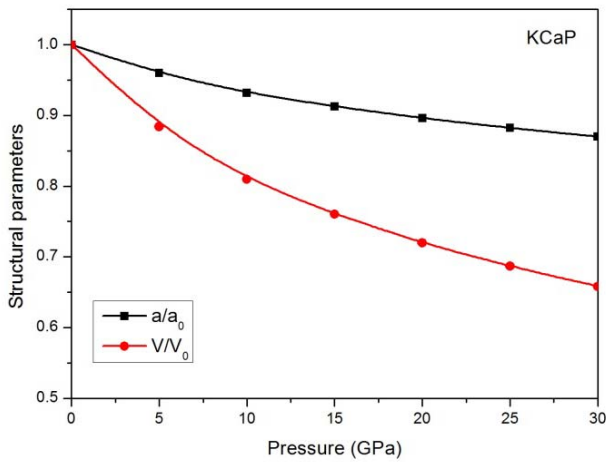


Fig. 2. The variation of structural parameters of KCaP compound ($C1_b$) under pressure

The variation of lattice constants and volume values of KCaP compound as 30 GPa pressure is illustrated in Figure 2. As the pressure value increases, the lattice constant is decreased as estimated. Obtained values from volume differences at various pressures are used to calculate volume collapse ($\frac{\Delta V}{V_0} \cdot 100$). Here ΔV is the

change in volume and V_0 is the equilibrium volume at zero pressure. The occurring volume collapses are calculated 11.57%, 19.01%, 23.96%, 28.04%, 31.32% and 34.19% from 5 GPa to 30 GPa, respectively. As pressure increases, volume collapse invariably increases for half-Heusler KCaP compound.

The *ab-initio* calculations are performed using density functional theory within the Perdew-Burke-Ernzerhof parametrization of the generalized gradient approximation (GGA) [10, 11] as implemented in the Vienna Ab-initio Simulation Package (VASP) [12-15]. For the plane-wave basis set, the kinetic energy cutoff is taken to be

$\hbar^2 |\vec{k} + \vec{G}|^2 / 2m = 600 \text{ eV}$. The numerical integration of Brillouin zone is applied using a $16 \times 16 \times 16$ Monkhorst-Pack k-points sampling procedure for KCaP

compound. The calculations of elastic properties under pressure effect are taken into account by ELAM code [16].

3. Results and discussion

3.1. Structural and elastic properties

The lattice parameters, volume, interatomic distances between each type of atoms, bulk modulus and compressibility with results of other reference calculations, are presented in Table 1.

Table 1. Lattice parameter (a), volume (V), interatomic distance (d), bulk modulus (B), compressibility (β)

a (Å)	V (Å ³)	d_{K-Ca} (Å)	d_{K-P} (Å)	d_{Ca-Ca} (Å)	B (GPa)	β (TPa ⁻¹)
7.220	376.367	3.610	3.126	5.105	30.59	7.92
7.201 ^a						
7.066 ^b					29.08 ^b	
7.212 ^c						

^a Ref. [5], numerical study using LAPW calculation and EV-GGA,

^b Ref. [7], numerical study using WIEN2K code and L/APW + lo method,

^c Ref. [8], numerical study using WIEN2K code PBE-GGA approximation and a modified version of the exchange potential TB-mbJ.

The present lattice constant is estimated to be 7.220 Å for KCaP compound. The calculated present lattice constant is good agreement with the other numerical studies. The present lattice constant in $C1_b$ -type crystal structure for half-Heusler KCaP compound is nearly 0.264% upper than the reference value [5], 2.179% upper than the reference value [7] and 0.111 upper than the reference value [8]. These fractionations may arise from the using of GGA approximations with different *ab-initio* codes and methods.

Taking the optimized structure as a reference, a series of constant volume structural optimizations have been proved in order to obtain energy versus volume changes that allow the determination of the equilibrium volume and the bulk modulus by fitting these data to the Murnaghan equation, appropriate for crystals at ambient pressure values [17]. The bulk modulus value of KCaP compound is in very good agreement with other numerical value of reference [7]. Additionally, interatomic distances are concerned and given in Table 1 as follow: distance of between K and Ca atoms is 3.610 Å, distance of between K and P atoms is 3.126 Å and distance of between Ca and Ca atoms is 5.105 Å; as it can be seen from Fig. 1.

The bulk modulus is the resistance of a material against volume variation of the system. Our bulk modulus is calculated as 30.59 GPa at zero pressure. Comparing

with reference [7] the modulus is found as 29.08 GPa calculated using by L/APW + lo method and very good convenient value (see Table 1). The compressibility is related with elastic constants [18]:

$$\beta = \frac{C_{11} - C_{12}}{\Omega} \quad (1)$$

Here $\Omega = (C_{11} + C_{12})C_{11} - 2C_{12}^2$. The pressure effects on the axial compressibility β is calculated as 7.92 TPa^{-1} and given in Table 1.

The elastic properties have a crucial role in providing valuable information about the binding characteristic between atomic planes. In the framework of our calculations of elastic properties, the second-order elastic constants (C_{ij}) are calculated using by “stress-strain method” [19, 20] at different pressure values from 0 to 30 GPa.

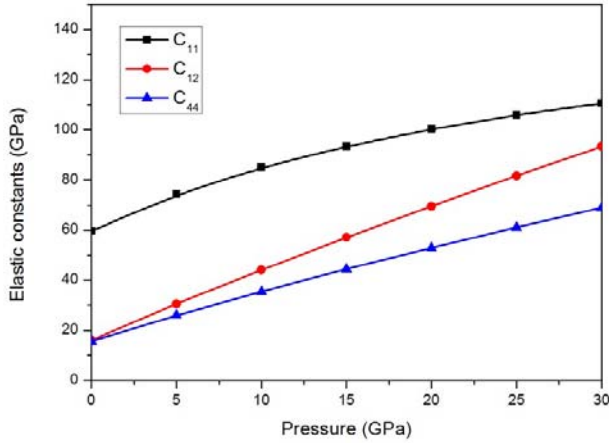


Fig. 3. Elastic constants for KCaP at different pressures

In Fig. 3, the variations of second order elastic constants with pressure dependences are presented. A linear dependence in all curves in the considered range of pressure (0 GPa-30 GPa) is clearly observed.

The elastic constants are evaluated with respect to Born's stability criteria that should be satisfied for the stability conditions of crystal lattice [21]. Known and substantial conditions for mechanical stability of cubic crystals are as follow: $C_{11} > 0$, $C_{11} - C_{12} > 0$, $C_{44} > 0$, $C_{11} + 2C_{12} > 0$ and $C_{12} < B < C_{11}$. According to Born's stability criteria, the half-Heusler compound KCaP in $C1_b$ structure is mechanically stable at zero pressure.

Consideration of cubic crystals under pressure P , the generalized elastic stability conditions are discussed with following equations [22, 23]:

$$\text{Condition 1: } K = 1/3(C_{11} + 2C_{12} + P) > 0 \quad (2)$$

$$\text{Condition 2: } G = C_{44} - P > 0 \quad (3)$$

$$\text{Condition 3: } G' = 1/2(C_{11} - C_{12} - 2P) > 0 \quad (4)$$

Where, K is isothermal bulk modulus, G is rhombohedral shear modulus and G' is tetragonal shear modulus. The calculated results are presented in Table 2 for three conditions.

Table 2. Mechanical stability of the half-Heusler KCaP compound under pressure

Pressure (GPa)	Condition 1	Condition 2	Condition 3
0	30.59	15.59	21.81
5	46.78	21.01	16.86
10	61.09	25.49	10.45
15	74.22	29.41	3.22
20	86.46	32.84	-4.58
25	98.12	36.09	-12.83
30	109.15	39.02	-21.39

The half-Heusler compound KCaP provides K and G conditions at different pressure values unlike G' condition. Tetragonal shear modulus of KCaP compound is calculated and is mechanically stable from 0 GPa to 20 GPa while it is unstable for higher than 15 GPa (see Table 2).

One of the distinct parameter is Kleinman parameter that describes the relative positions of the cation and anion sublattices under volume conserving strain distortions for which positions are not fixed by symmetry [24]. Kleinman parameter is defined as below relation:

$$\xi = \frac{C_{11} + 8C_{12}}{7C_{11} + 2C_{12}} \quad (5)$$

The pressure dependence of Kleinman parameter is also evaluated for the half-Heusler KCaP compound and shown in Fig. 4.

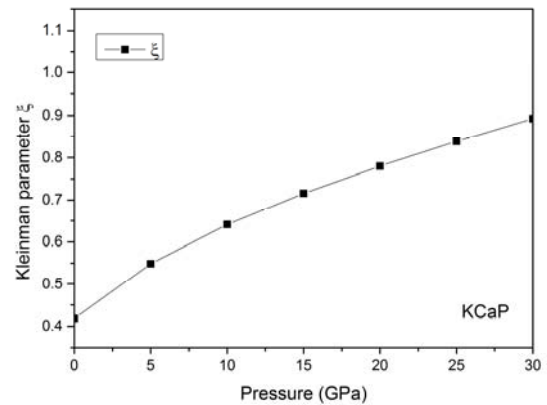


Fig. 4. Kleinman parameter of KCaP at different pressures

As the pressure increases linearly, Kleinman parameter of the half-Heusler KCaP compound is reached to high values.

Additionally, anisotropic features of binding and structural stability are usually defined by the elastic constants that have been related to the shear modulus G and Young modulus E .

The anisotropic behaviors are changed by applied increasing pressure. Analysis of the stiffness constants under pressure reveals highly anisotropic elastic behavior. The analysis of anisotropic elastic properties is calculated by using EIAM code [16]. We have also included the $A_E = E_{max}/E_{min}$ of the anisotropy factor of Young's modulus, and A_G of the anisotropy factor of shear modulus (see Table 3).

Table 3. Maximal and minimal values of anisotropic factors (E: Young and G: shear modulus)

P(GPa)	E_{max} (GPa)	E_{min} (GPa)	A_E	G_{max} (GPa)	G_{min} (GPa)	A_G
0	52.86	39.98	1.323	0.0218	0.0156	1.397
5	65.45	56.46	1.159	0.026	0.0219	1.187
10	88.36	54.87	1.610	0.0355	0.0205	1.732
15	109.74	50.24	2.184	0.0444	0.0182	2.439
20	129.83	43.46	2.987	0.0528	0.0154	3.429
25	149.34	34.95	4.273	0.0611	0.0122	5.008
30	167.96	25.12	6.686	0.069	0.0086	8.023

The minimal and maximal values of Young's modulus under pressure are mentioned in Table 4 between 0-30 GPa pressure values. Young's modulus is revealing rigidity of compounds. There is a sharp contrast with the behavior of Young's modulus of KCaP after 15 GPa. A_E values are similar with each other until 15 GPa and the values of Young's modulus in their direction of highest rigidity. After this pressure, minimal value of Young's modulus is beginning to decrease and anisotropy is broken.

The shear modulus G of this framework is obtained at different pressures and calculated the minimal and maximal values as a function of direction (θ , φ). We conclude that shear modulus anisotropy has immense values with increased pressures while it has negligible values at low pressures.

The anisotropy factor, A , has been calculated to understand the elastic anisotropy of KCaP. It has been recommended [25] that big values of A can present revealed to the tangential force move to screw dislocations to improve the cross-slip formations. The condition for the cross-slip formation model [26] is $[3A/(A+2)]\gamma_1/\gamma_0 > 3^{1/3}$, where γ_1 and γ_0 are the anti-phase boundary energies of the $\{111\}$ and $\{100\}$ planes, respectively. As a matter of fact, the notionally high anisotropy factor $A (>2)$ is prone to elastically increase to the cross slip. The anisotropy of the crystal is measured by the symmetry plane and axis. The anisotropy factors are calculated from elastic constants using by relations 6 and 7:

$$A^{[001],(100)} = \frac{2C_{44}}{C_{11} - C_{12}} \quad (6)$$

$$A^{[001],(110)} = \frac{C_{44}(C_l + 2C_{12} + C_{11})}{C_{11}C_l - C_{12}^2} \quad (7)$$

Where C_l is $C_l = C_{44} + (C_{11} + C_{12})/2$ the $[ijk]$ and (ijk) indicate symmetry axis and plane, respectively.

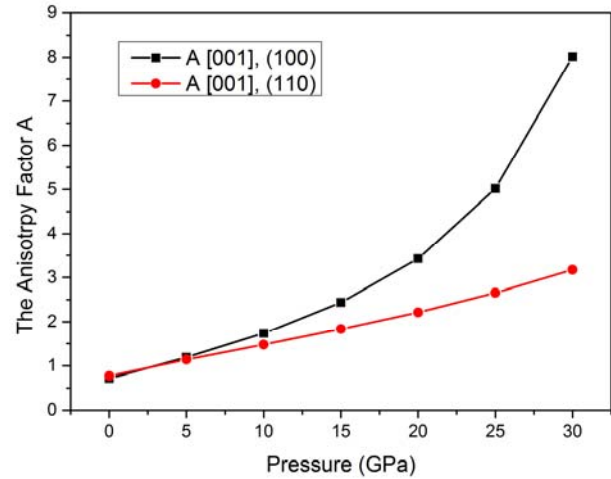


Fig. 5. The anisotropy factor of KCaP at different pressures

The calculated anisotropy factors are given in Table 3 at different pressure values and illustrated in Fig. 5 with respect to axis and planes. Anisotropy factors of half-Heusler KCaP compound are increase linearly to 10 GPa, more than 10 GPa pressure value the anisotropies raise the cross-slip formation.

The Poisson's ratio, σ , characterizes the stability of the crystal against shearing strain. Considering the typical alloys, this value will have been changed according to directions. Our values of The Poisson's ratio, σ , for two main cubic directions $[001]$ and $[111]$ directions defined as using the second-order elastic constants [27]:

$$\sigma^{[001]} = \frac{C_{12}}{C_{11} + C_{12}} \quad (8)$$

$$\sigma^{[111]} = \frac{C_{11} + 2C_{12} - 2C_{44}}{2(C_{11} + 2C_{12} + C_{44})} \quad (9)$$

The calculated Poisson ratios according to directions are $\sigma^{[001]}=0.21$ and $\sigma^{[111]}=0.28$ at zero pressure. The pressure dependence of the Poisson's ratios of KCaP along the main directions is plotted in Figure 6.

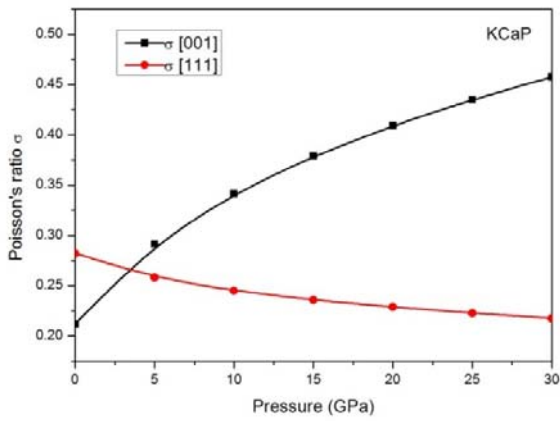


Fig. 6. The Poisson's ratio of KCaP at different pressures

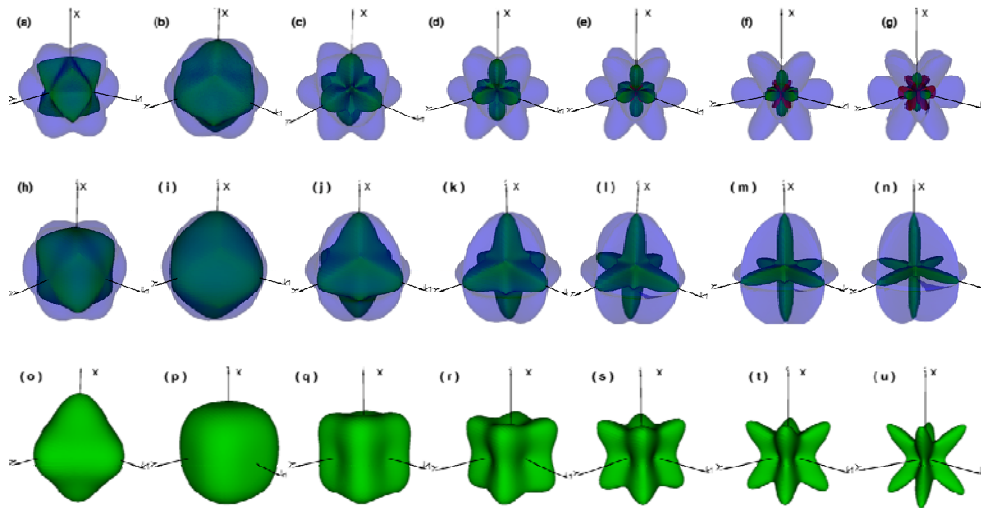


Fig. 7. 3D directional dependence of the Poisson's ratio (a-g), shear modulus (h-n) and Young's modulus (o-u) of KCaP compound

The Poisson's ratio is evaluated under pressure and also mentioned to the directional with Figure 6. As shown in Figure 7 (a-g), x-axis of Poisson's ratio is more compressible than the y and z-axis.

The shear anisotropic factors are obtained by Eq.s 6 and 7 and evaluated with increasing pressure in Figure 5 and Table 3. Similarly, the shear anisotropy has larger values more than 10 GPa (see Figure 7.j). The anisotropy of shear modulus is increasing along the x-axis otherwise the anisotropy of Young's modulus.

When the pressure is 0 GPa, it can be seen that the 3D figure of the Young's modulus of half-Heusler KCaP compound has a larger deviation in shape after 10 GPa (see Figure 7.q). This deviation is increasing with pressure that is plotted in Figure 7.u. The elastic anisotropic results obtained from the 3D figures of the Young's modulus are consistent with the analysis of anisotropic behaviors (see Table 3).

The Poisson's ratio gives the information about bonding forces of elastic constants [28]. The interatomic forces present strong forces in the bonding in [111] direction. Reasonable slight increase of $\sigma^{[001]}$ and $\sigma^{[111]}$ could be seen with increasing pressure. The Poisson's ratio in [111] direction decreases while the Poisson's ratio in [001] direction increases with increasing pressure. The elastic anisotropy behavior of half-Heusler KCaP compound is described by the three-dimensional (3D) surface construction in Fig 7.

As shown in Fig. 7, directional dependence of the Poisson's ratio (a-g), shear modulus (h-n) and Young's modulus (o-u) of KCaP compound are depicted from 0 GPa to 30 GPa, respectively by fives. The EIAM code [16] is performed to visualize three-dimensional Poisson's ratio, shear and Young's modulus.

3.2. Electronic properties

The electronic structure of half-Heusler KCaP compound is investigated by computing the band structures with total and partial density of states that are depicted in Figures 8 and 9 at equilibrium lattice constant.

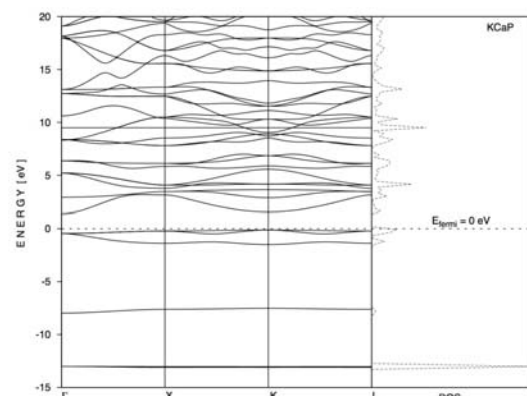


Fig. 8. Electronic band structure of KCaP

The calculated band structure along the high symmetry directions of the Brillouin zone for half-Heusler KCaP compound is shown in Figure 8. It can be seen that KCaP is a direct band gap material with a band gap of 1.559 eV at zero pressure. In the band structures, the top of valance band and the bottom of the conduct band are located at *K*-point is clearly observed. The Fermi energy is set to zero. The pressure dependence of band gap with Fermi energies is given in Table 4.

Table 4. Band gaps with Fermi energy levels under pressure

Pressure (GPa)	Band gap (eV)	Fermi energy (eV)	Direct gap
5	1.557	1.277	K-K
10	1.454	1.595	K-K
15	1.354	2.039	K-K
20	1.257	2.346	K-K
25	1.164	2.597	K-K
30	1.076	2.906	K-K

As it is seen from Table 4, band gap decreases while the pressure values decrease. For all pressure values, the half-Heusler KCaP compound has direct band gap.

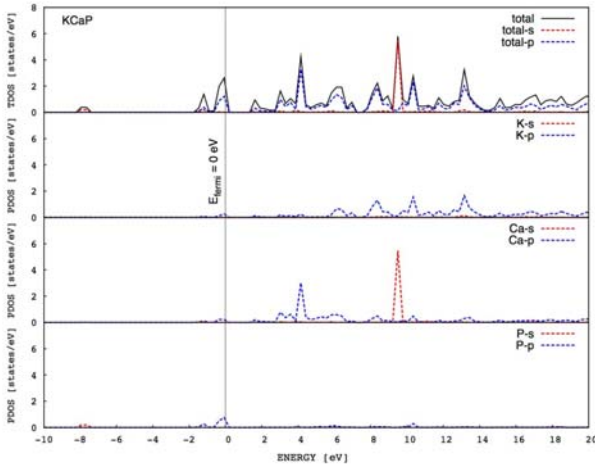


Fig. 9. Total and partial density of states of KCaP

The density of states (DOS) of a system describes the number of states at each energy level, which is available to be occupied in solid state physics. We have presented the total density of states (TDOS) and partial density of states (PDOS) of KCaP in Figure 9. As is clearly shown in Fig. 9, under the conventional GGA model, the contribution to the lower valance bands are mainly P-3s states (located at -8 eV), the middle valance bands are mainly the P-2p states (located at -2 ~ -1.5 eV) and the upper valance bands are dominated by P-3p states and Ca-2p states (located at -1 – 0 eV). The calculated whole width of valance band is 10 eV. The conduction bands are mainly from Ca-s states and K-p states, partially Ca-p states. Ca-s states have a maximum nearly at 9 eV. The half-Heusler KCaP

compound has a semiconducting behavior due to the fact that it has band gap.

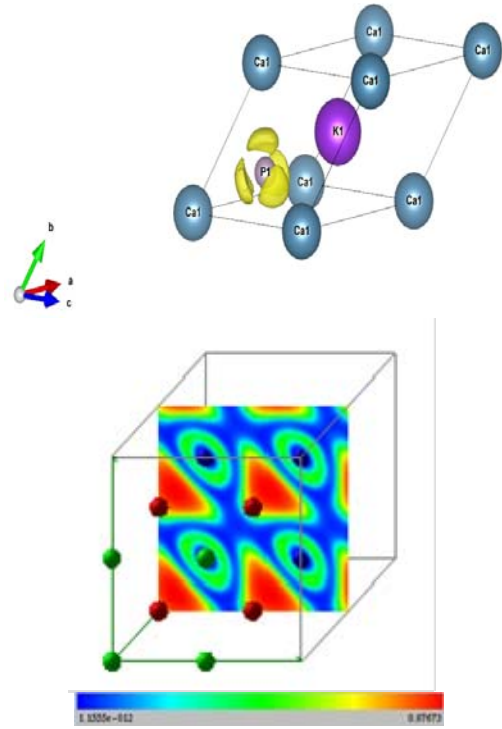


Fig. 10. a. Charge density isosurfaces b. Charge density contours of KCaP compound

The charge density iso-surfaces of KCaP compound is plotted in Figure 10.a. P has a certain isosurface because of its valance electrons. The red spheres are potassium (K), the green spheres are calcium and the blue ones are phosphorous (P). According to Figure 10.b, the localization of charge density around the Ca atom is more obvious than P atoms. We note that the core regions of Ca atoms have the largest charge density, which is mainly due to ionic core orbitals. In addition, the electron accumulation between the neighboring P atoms shows the existence of covalent bonding, while the near-spherical charge distributions around K atoms indicate a metallic bonding. The charge density between K and P atoms is slightly higher than that of the Ca and P atoms is also observed that results in the higher bonding strength for K-P bonding.

3.3. Optical properties

We have also discussed the optical properties of half-Heusler KCaP compound due the fact that it is demonstrated as optoelectronic devices. The optical properties of a solid material are usually described by the complex dielectric function $\epsilon(\omega) = \epsilon_1(\omega) + i\epsilon_2(\omega)$. The complex dielectric function characterizes the linear response of the material to an electromagnetic radiation. The imaginary part of dielectric function $\epsilon_2(\omega)$ represents the optical absorption in the crystal. $\epsilon_2(\omega)$ can be calculated using by the momentum matrix elements

between the occupied and unoccupied wavefunctions. The real part of dielectric function $\varepsilon_1(\omega)$ is calculated using Kramer–Kronig relations. The real part of dielectric function is found the following relation in where M is the principle value of the integral:

$$\varepsilon_1(\omega) = 1 + \frac{2}{\pi} M \int_0^{\infty} \frac{\varepsilon_2(\omega') \omega'}{\omega'^2 - \omega^2} d\omega' \quad (10)$$

The imaginary part of the dielectric function is calculated from the matrix elements as following relation:

$$\varepsilon_2(\omega) = \frac{Ve^2}{2\pi m^2 \omega^2} \int d^3k \sum_{n,n'} \left| \langle kn | p | kn' \rangle \right|^2 f(kn) (1 - f(kn')) \delta(E_{kn} - E_{kn'} - \hbar\omega) \quad (11)$$

where V is the volume of the unit cell, e is the electron charge, m is its mass, $|kn\rangle$ is the wave function of the crystal, $f(kn)$ is the Fermi-Dirac function distribution, $\hbar\omega$ is the incident photon energy, n refers the unoccupied wave functions and n' refers the occupied wave functions.

$L(\omega)$ are given respectively as following relations (12-15) [29, 30]:

$$n(\omega) = \left(\frac{\varepsilon_1(\omega)}{2} + \frac{\sqrt{\varepsilon_1^2(\omega) + \varepsilon_2^2(\omega)}}{2} \right)^{1/2} \quad (12)$$

$$k(\omega) = \left(\frac{\sqrt{\varepsilon_1^2(\omega) + \varepsilon_2^2(\omega)} - \varepsilon_1(\omega)}{2} \right)^{1/2} \quad (13)$$

$$R(\omega) = \left(\frac{(n(\omega) - 1)^2 + k(\omega)^2}{(n(\omega) + 1)^2 + k(\omega)^2} \right) \quad (14)$$

$$L(\omega) = \left(\frac{\varepsilon_2(\omega)}{\varepsilon_1^2(\omega) + \varepsilon_2^2(\omega)} \right) \quad (15)$$

By using these relations, the determined optical parameters are plotted in Fig. 12.

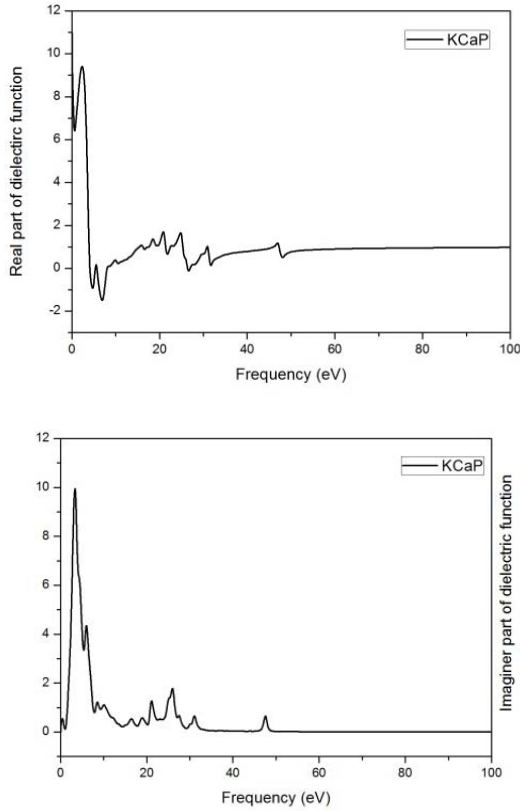


Fig. 11. a. Real part of dielectric function b. Imaginary part of dielectric function

Fig. 11 shows the calculated dielectric function of half-Heusler KCaP compound. It can be seen that the imaginary spectrum of $\varepsilon(\omega)$ has a prominent absorption peak, located at the photon energy of nearly 5 eV.

The expressions of optical properties using by dielectric functions, refractive index $n(\omega)$, extinction coefficient $k(\omega)$, reflectivity $R(\omega)$ and energy loss function

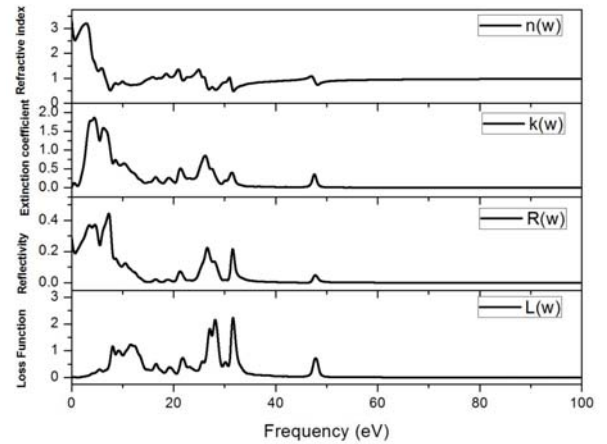


Fig. 12. Refractive index $n(\omega)$, extinction coefficient $k(\omega)$, reflectivity $R(\omega)$ and energy loss function $L(\omega)$ of KCaP compound

According to the dispersion curve of refractive index at $\omega=0$, $n(\omega)$ is found to be 3.01. The extinction coefficient ($n(\omega)$) is estimated as 3.60. Reflectivity has less peak values in contrast to loss function. The main peak as it is known plasmon frequency (ω_p) is evaluated in the energy loss functions $L(\omega)$. Two main peaks are in the energy loss function spectrum. But, one of them is higher and is located at nearly 32 eV.

4. Conclusions

The first-principles calculations have been carried out of the structural, anisotropic elastic properties, electronic properties and optical properties of half-Heusler KCaP compound. The obtained results have shown that the half-Heusler KCaP compound is mechanically stable in considered structure. The mechanical stability and elastic anisotropy is also considered and presented under pressure effect. The pressure dependence increases, the anisotropy increases. The elastic parameters have been calculated by Voigt-Reuss-Hill approximation. The electronic properties are investigated not only band structure calculations, but also charge densities are given with bonding character. The half-Heusler KCaP compound exhibits a semiconducting behavior.

Acknowledgement

Y. Mogulkoc acknowledges Ankara University for financial support under AYP with 17A0443001 project number.

References

- [1] F. Casper, T. Graf, S. Chadov, B. Balke, C. Felser, *Semicond. Sci. Technol.* **27**, 063001 (2012).
- [2] N. Shutoh, S. Sakurada, *Journal of Alloys and Compounds* **389**, 204 (2005).
- [3] H. Muta, T. Kanemitsu, K. Kurosaki, S. Yamanaka, *J. Alloys Compounds* **469**, 50 (2009).
- [4] W. Xie, A. Weidenkaff, X. Tang, Q. Zhang, J. Poon, T. M. Tritt, *Nanomaterials* **2**, 379 (2012).
- [5] D. Kieven, R. Klenk, *Phys. Rev. B* **81**, 075208 (2010).
- [6] T. Gruhn, *Phys. Rev. B* **82**, 125210 (2010).
- [7] H. Mehnane, B. Bekkouche, S. Kacimi, A. Hallouche, M. Djermouni, *Superlattices and Microstructures* **51**, 772 (2012).
- [8] S. Kacimi, H. Mehnane, A. Zaoui, *Journal of Alloys and Compounds* **587**, 451 (2014).
- [9] C. Kandpal, C. Felser, R. Seshadri, *J. Phys. D* **39**, 776 (2006).
- [10] J. P. Perdew, K. Burke, M. Ernzerhof, *Phys. Rev. Lett.* **77**, 3865 (1996).
- [11] J. P. Perdew, K. Burke, M. Ernzerhof, *Phys. Rev. Lett.* **78**, 1396 (1997).
- [12] G. Kresse, J. Hafner, *Phys. Rev. B* **47**, 558 (1993).
- [13] G. Kresse, J. Hafner, *Phys. Rev. B* **49**, 14251 (1994).
- [14] G. Kresse, J. Furthmüller, *Comput. Mat. Sci.* **6**, 15 (1996).
- [15] G. Kresse, J. Furthmüller, *Phys. Rev. B* **54**, 11169 (1996).
- [16] A. Marmier, Z. A. D. Lethbridge, R. I. Walton, C. W. Smith, S. C. Parker, K. E. Evans, *Computer Physics Communications* **181**, 2102 (2010).
- [17] F. D. Murnaghan, *Proc. Natl. Acad. Sci. USA* **30**, 244 (1944).
- [18] J. F. Nye, *Physical properties of crystals: their representation by tensors and matrices*, Oxford, Clarendon, 1985.
- [19] L. Page, P. Saxe, *Phys. Rev. B* **65**, 104104 (2002).
- [20] M. J. Mehl, J. E. Osburn, D.A. Papaconstantopoulos, B. M. Klein, *Phys. Rev. B* **41**, 10311 (1990).
- [21] M. Born, K. Huang, *Dynamical Theory of Crystal Lattices*, Clarendon Press (1956).
- [22] S. Yip, J. Li, M. Tang, J. Wang, *Materials Science and Engineering* **A317** 236 (2001).
- [23] G. V. Sinko, N. A. Smirnov, *J. Phys.: Condens. Matter* **14**, 6989 (2002).
- [24] W. A. Harrison, *Electronic Structure and Properties of Solids*, New York: Dover (1989).
- [25] M. H. Yoo, *Scr. Metall.* **20**, 915 (1986).
- [26] S. Takeuchi, E. Kuramoto, *Acta Metall.* **21**, 415 (1973).
- [27] M. Friak, M. Sob, V. Vitek, *Philos Mag.* **83**, 3259 (2003).
- [28] W. Koster, H. Franz, *Metall. Rev.* **6**, 1 (1961).
- [29] Y. Shen, Z. Zhou, *J. Appl. Phys.* **103**, 074113 (2008).
- [30] M. Dadsetani, A. Pourghazi, *Phys. Rev. B* **73**, 195102 (2006).

*Corresponding author: mogulkoc@eng.ankara.edu.tr